EDFAAO (2005) 4:24-31 1537-0755/$19.00

Quantitative Analysis and Depth Measurement via Magnetic Field Imaging

Benaiah D. Schrag,* Xiaoyong Liu,* Jan S. Hoftun,* Peter L. Klinger,**
T.M. Levin,** and David P. Vallett**
*Micro Magnetics, Inc., Fall River, Mass.
**IBM Systems and Technology Group, Essex Junction, Vt.
schrag@micromagnetics.com

Introduction

Over the past several years, magnetic field imaging[1-3] has been gaining popularity as a technique for fault isolation in integrated circuits and semiconductor packages. One important advantage of this method is that magnetic fields due to electrical currents can be measured through most materials typically found in ICs or packages. Therefore, magnetic field imaging is used as a noninvasive way to visualize current throughout an IC or package without the need for expensive and time-consuming sample preparation or decapsulation.

The raw data acquired during a magnetic field scan is a field strength map of a single component (usually the out-of-plane component) over the area scanned. Generally, the information provided by a successful magnetic imaging session is a map of current densities in the conductive planes of the device under test (DUT). Examples of a typical magnetic field map and the corresponding current density map are shown in Fig. 1 and 2. In many cases, such a map is overlaid on an optical or CAD image of the DUT, and the resulting information is sufficient to localize the fault. However, as is shown in this article, the same magnetic field data that are used to produce the current density map can also be analyzed to provide a variety of important quantitative parameters about the DUT itself. These parameters include the exact current, depth (and therefore the metal level), and, in some cases, the width of each conductor found in the current density map. In this experiment, the authors explain how depth is easily extracted from a magnetic field scan. It is the authors' belief that the ability to measure these parameters, in particular the current depth, is unique among mainstream fault isolation methods and will greatly assist in the failure analysis process.

Magnetic Field Imaging: Theory

It has been known since the 1800s that any electrical current creates a localized magnetic field in its vicinity. The Biot-Savart Law of electromagnetism

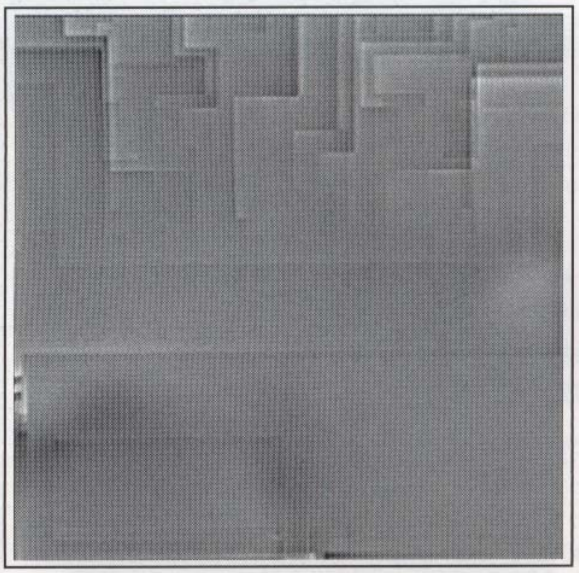

Fig. 1 Sample magnetic field map acquired at the surface of an operating IC

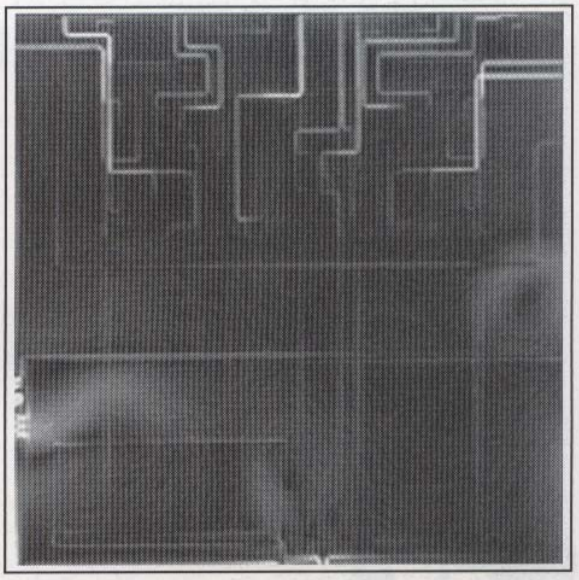

Fig. 2 Current density map calculated from the magnetic field data in Fig. 1

quantifies this relationship between the current and the magnetic field:

$$\vec{B} = \frac{\mu_0 I d\vec{L} \times \hat{r}}{4\pi r^2} \qquad \text{(Eq 1)}$$

where B is the magnetic field, μ_0 is the permeability of free space, I and dL indicate the magnitude and direction of an infinitesimal segment of current, and r is the vector between the sensor and the current segment. Building on Eq 1, the magnetic field a distance r away from an infinitely long, straight, thin conductor carrying a current I is given by:

$$\vec{B} = \frac{\mu_0 I}{2\pi r} \hat{\phi} \qquad \text{(Eq 2)}$$

where ϕ is the position vector in polar coordinates. Finally, a conductor with a finite width $2d$—which is a good approximation to most current paths in semiconductor chips and packages—creates a magnetic field profile whose z-component is given by:

$$B_z(x, y, z) = \frac{\mu_0 I}{8\pi d} \log\left(\frac{z^2 + (x+d)^2}{z^2 + (x-d)^2}\right) \qquad \text{(Eq 3)}$$

where B_z is the x-component of the magnetic field at a three-dimensional position (x, y, z), z is the vertical distance between the conductor and the sensor, and it is assumed that the conductor runs in the y-direction. (Therefore, Eq 3 describes the magnetic field profile that will be observed when moving in the direction perpendicular to the direction of current.) As will be shown, Eq 3 forms the basis for the extraction of quantitative information from magnetic field scans of ICs. Contained in Eq 3 are three unknown parameters: I, the current amplitude; d, the half-width of the conductor; and z, the vertical distance between the sensor and the conductor. Figure 3 shows the shape of the previously mentioned profile for $I = 100$

(continued on page 26)

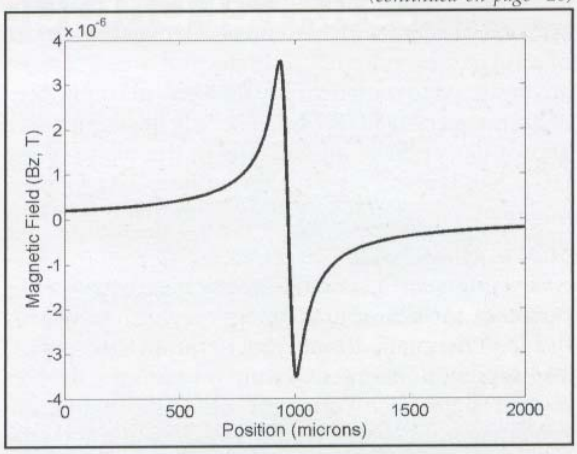

Fig. 3 *The characteristic two-peaked magnetic field profile of a current-carrying conductor*

μA, $d = 25$ μm, and $z = 25$ μm. While the exact shape of the curve varies with the aforementioned parameters, all single conductors create the distinctive two-peaked field signature seen in Fig. 3. Variations in each of these three parameters will create distinct changes in the shape of the measured magnetic field profile. The quantitative capability takes advantage of this fact.

Magnetic Field Imaging: Details

Magnetic field imaging is typically conducted using a scanning probe methodology, where a magnetic sensor is rastered with high precision over the surface of a current-carrying DUT. In general, these sensors are designed to measure only the vertical component of the magnetic field (B_z), because only this component allows detection of all currents in the plane of the DUT. This is also the reason the authors have focused on only the z-component of the field in the previous discussion.

Several sensor technologies have been used for this purpose, including giant magnetoresistive (GMR) heads,[3] magnetic tunnel junction (MTJ) sensors,[3] and superconducting quantum interference devices (SQUIDs).[1,2] Each variety of sensor has a different sensitivity and spatial resolution, depending on the physical size of the sensor and on the sensing methodology.

All of the measurements in this experiment were made with a Circuit Scan CS1000 imaging system (Micro Magnetics, Inc., Fall River, Mass.). This system uses both GMR and MTJ sensing elements. While the methods presented herein apply equally well to any sensor technology, all measurements made for this work used an MTJ sensor[4,5] to take advantage of its excellent combination of spatial resolution (~1 μm) and current sensitivity (~125 nA/rtHz). All data analysis was accomplished using a data analysis routine designed specifically for depth measurement.

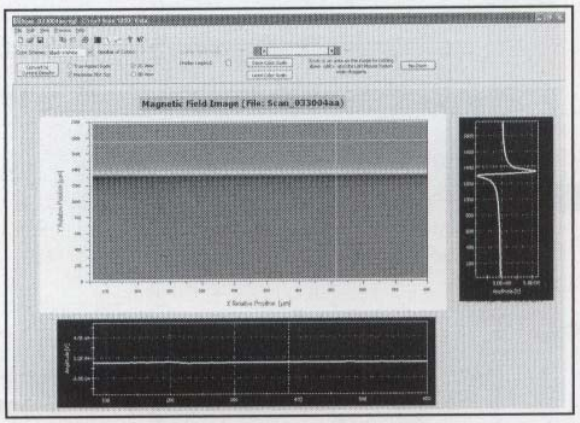

Fig. 4 Screenshot showing the magnetic field map (center) and projections (bottom and right) to be analyzed

Quantitative Analysis and Depth Measurement: Procedure

Figure 4 shows a simple magnetic field map acquired at the surface of a device, with a single current path running horizontally. In this field map, a false grayscale is used such that white and black represent large positive and large negative field values, respectively. At the right and bottom of the figure are horizontal and vertical projections of the field map. It is these projections that are used to do quantitative analysis. The characteristic field profile described previously can be seen in the projection to the right of the field map.

Once a particular projection is identified, it is analyzed using a dialog, as shown in Fig. 5. This screen consists of a graph of the selected projection, below which are several groups of text boxes, with each group corresponding to a particular numerical parameter. In addition to the three unknown parameters—I, d, and z—described previously, there are also parameters representing the overall position of the center of the conductor and the overall magnetic field baseline. These two parameters can be thought of as "offsets" in the horizontal and vertical directions. The field projection in Fig. 5 contains magnetic field signatures from two separate current paths, which is the reason for two sets of peaks in the data.

The basic idea behind the analysis process is to find the theoretical curve based on Eq 3 that best fits the data in the projection. In the case of a projection containing multiple field signatures, such as that in

(continued on page 28)

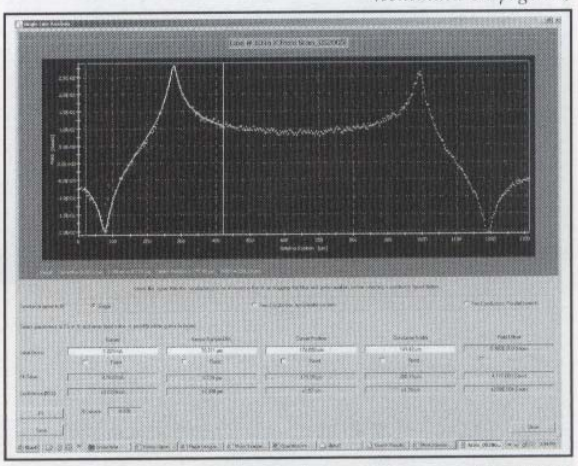

Fig. 5 Screenshot of the quantitative analysis screen. The fitted curve (solid white line) is displayed over the data from the magnetic field projection (white dots).

Fig. 5, a pair of sliders (shown) is used to select a particular section of the data for the analysis. It is important to note that the fitting process only requires a single one-dimensional line of data that is a subset of the two-dimensional magnetic field map. The analysis routine uses a Levenberg-Marquardt iterative curve-fitting process.[6] The function is designed to allow input of as much or as little prior information about the current path being analyzed as is known. In order to do this, three options with respect to each parameter are given:

- The parameter can be fixed at a known value (for example, if one knows the current amplitude in the conductor being analyzed).
- An initial guess for the parameter can be entered, after which it is allowed to vary during the fitting process.

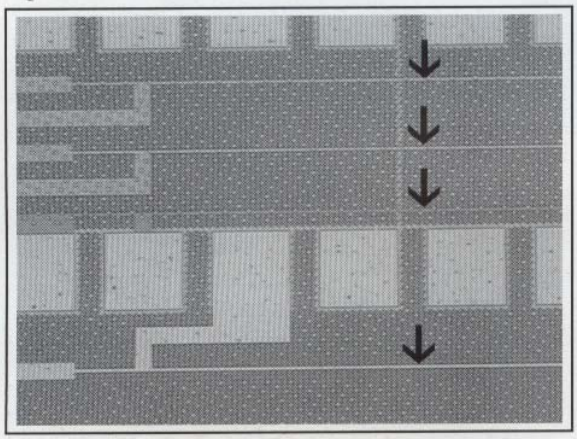

Fig. 6 *Four-wire test structure with conductors at four different metal levels used in the experiment (arrows indicate the individual wire segments on each level)*

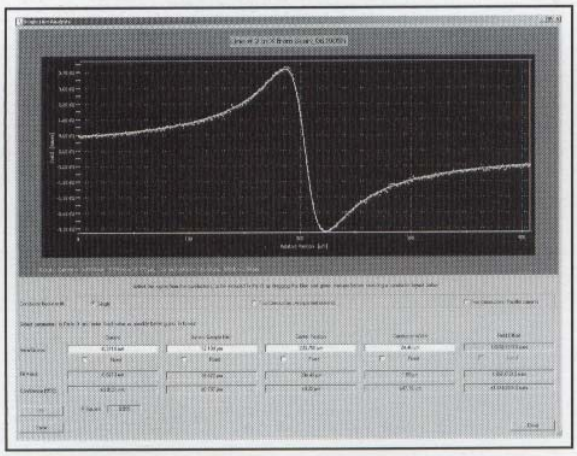

Fig. 7 *Good agreement (R = 0.995+) was observed in all cases for the analysis of the four-level test structure. Dots indicate the magnetic field data, with the best-fit curve represented by a solid line.*

- The software will automatically make an initial guess based on an analysis of the data.

The results of this process are shown in Fig. 5. After the fitting process is complete, the best-fit theoretical curve is overlaid on top of the data so that one can visually check how well the two curves match. In the graph, the white dots indicate the experimental data, while the solid line is the best-fit curve. The agreement between the two curves is quantified by the *R*-value (correlation coefficient) of the fit, given at the bottom right, where *R* ranges from 0 to 1, with $R = 1$ indicating perfect agreement. The *R*-value for the fit in Fig. 5 is 0.998.

All of the best-fit parameters—including *I*, *d*, and *z*—are given in boxes below the graph, along with estimates of their uncertainty, as shown in Fig. 5.

Case Study

In order to demonstrate the effectiveness of quantitative analysis, a series of scans was conducted on a four-level metal test structure, as shown in Fig. 6. The section of the sample that was imaged contained four conductors at four different metal levels, each of which could be powered independently. Four magnetic field images were acquired, each with a different conductor excited with an ~700 μA_{rms} signal. Each field map took approximately 1 min to acquire, and each featured a signal-to-noise ratio of approximately 100. Every magnetic field map consisted of three horizontal lines of data, each of which was then analyzed separately. While the fitting process only requires a single line of data, the collection of three lines allowed the authors to ensure that the data were self-consistent. The sample current was measured and recorded before each scan; however, no such sample or powering details were used at any point of the data analysis.

The initial set of scans was made in light contact mode, where the sensor probe follows the contour of the sample surface with a small contact force. After this analysis was completed, the entire process was repeated in noncontact mode, where the sensor follows the contour of the sample surface from a known distance (in this case, ~3 µm). The resulting values obtained from each of the three lines of data in each scan were self-consistent to within 3 µA (for *I*) and 0.5 µm (for *z*).

Figure 7 shows the excellent agreement between the data (white dots) and the best-fit line (solid line) for a typical scan, with an *R*-value of 0.998. A summary of the results of the quantitative analysis process is shown in Table 1. The extracted current values are

approximately 2% below the actual measured values in each case. This systematic error is due to a slight error in the calibrated sensitivity of the MTJ sensor and can likely be corrected with a simple recalibration of the sensor.

The extracted values of the z parameter give the distance between the sensor area and the current path. Therefore, the z parameter is actually the sum of two components: (1) the distance between the surface of the sample and the sensor's active area, and (2) the distance between the sample surface and the current path (which can be thought of as the true "depth" of the current path). The sensor-to-surface component is calculated during the sensor calibration process (values are typically 5 to 7 μm) and is automatically subtracted during the analysis process. In the results listed in Table 1, the center of the top metal level (M4) has been used as a reference ($z = 0$).

In order to check the extracted depth results, a polished cross section was made on a similar die from the same batch, and an SEM was used to make depth measurements. The vertical distance between layers was assumed to be equal to the center-to-center distance between conductors in the cross section. Dimensions from the SEM along with the fitted dimensions are shown in Fig. 8 and Table 1, respectively. For the results obtained in light contact mode, the disparity between the two sets of values is less than 0.2 μm in every case, indicating excellent agreement. The results in noncontact mode are off by an average of 0.5 μm. This error is possibly due to the finite resolution (0.5 μm) of the vertical motion of the sensor. Another possible source of error is the assumption that the current is uniform over the thickness of each metal level. However, in either case, the accuracy (<0.5 μm) with which the current depth is determined is good enough to be able to distinguish between different metal levels in the vast majority of IC devices.

The values of d, the half-width of each conductor, could not be calculated in this case, for reasons that are explained in the following section.

Discussion

The authors have found that in almost all cases, the values of I and z can be determined accurately with percent errors similar to those noted previously. The half-width parameter (d) is more complicated. Numerical simulations were conducted, and it was found that as a general rule, the value of d can be determined only when d is significantly larger than z. The larger the ratio d/z, the more accurately the value of d can be pinned down. For example, the two curves in Fig. 5 were created by a different DUT containing two antiparallel conductors with $d = 100$ μm and $z = 8.5$ μm, while the curve-fitting results shown yielded $d = 100.10$ μm and $z = 8.3$ μm.

The quantitative analysis procedure relies on a few assumptions, which are important to keep in mind.

First, the theoretical formula used as an input for fitting represents an infinitely long current path. For any real sample, this assumption does not hold, but the authors have found that for segments where the length of the current path is more than ~8 to 10 times the sensor-to-sample distance (which is typically ~5 to 7 μm for frontside analysis, plus the thickness of any intervening sensor packaging for an MTJ), the error induced is negligible.

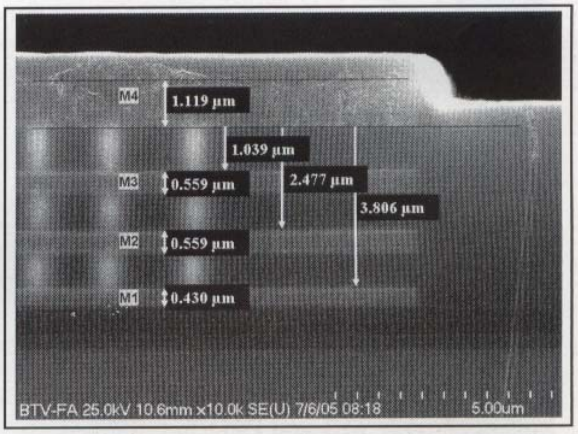

Fig. 8 Cross-sectional SEM imaging was used to measure the actual depths of each metal layer for comparison with the values calculated from the magnetic field profiles.

Table 1 Summary of results for the four-level test structure

Metal level	Actual current, μA	Extracted current, μA	Measured depth from SEM, μm	Extracted depth, μm (light contact)	Extracted depth, μm (noncontact)
M4	729 ± 10	714 ± 14	0**	0**	0**
M3	709 ± 10	697 ± 14	1.87	1.7 ± 0.2	1.5 ± 0.5
M2	608 ± 10	668 ± 14	3.32	3.4 ± 0.2	2.9 ± 0.4
M1	710 ± 10	699 ± 14	4.58	4.6 ± 0.2	3.7 ± 0.6

The second caveat is that the technique, as currently implemented, only works for conductors running vertically or horizontally with respect to the scan axes (which are set by the motion control system used to scan the sensor probe). For most currents in the die, this assumption holds true, but the analysis suite could be expanded to accommodate conductors running at all angles. For conductors at a small angle θ with respect to the vertical or horizontal, the extracted values of d and z will be too high by a factor of $1 - \sec(\theta)$. For angles of 5 and 10°, the magnitude of this error will be 0.3 and 1.5%, respectively.

Finally, this method assumes that one can select a portion of the field map whose field signature contains no magnetic interferences from nearby conductors. This problem can be minimized to some extent by a careful choice of the section of field map to be analyzed (using the two sliders, as in Fig. 5). However, in many cases, interference is an issue, and it remains to be investigated how "isolated" a conductor needs to be to obtain accurate results. One can bend this rule by fitting some special cases, such as two nearby conductors with parallel or antiparallel currents. The analysis could also be enhanced to deal with this issue.

References

1. S. Chatraphorn, E.F. Fleet, F.C. Wellstood, L.A. Knauss, and T.M. Eiles: "Scanning SQUID Microscopy of Integrated Circuits," *Appl. Phys. Lett.*, 2000, *76*(16), pp. 2304-06.
2. D.P. Vallett: "Scanning SQUID Microscopy for Die Level Fault Isolation," *Proc. 28th Int. Symp. Test. and Failure Analysis (ISTFA)*, Nov. 2002.
3. B.D. Schrag: "Scanning Magnetoresistive Microscopy for Die-Level Sub-Micron Current Density Mapping," *Proc. 29th Int. Symp. Test. and Failure Analysis (ISTFA)*, Nov. 2001, p. 2.
4. X. Liu, C. Ren, and G. Xiao: "Magnetic Tunnel Junction Sensors with Hard-Axis Bias Field," *J. Appl. Phys.*, 2002, *92*(8), pp. 4722-25.
5. X. Liu and G. Xiao: "Thermal Annealing Effects on Low-Frequency Noise and Transfer Behavior in Magnetic Tunnel Junction Sensors," *J. Appl. Phys.*, 2003, *94*(9), pp. 6218-20.
6. See, for example, *Numerical Recipes in C*, Cambridge University Press, Cambridge, U.K., 1992, pp. 656-99.

About the Authors

Ben Schrag is the project manager of metrology systems at Micro Magnetics. He received his B.A. in physics from Reed College in 1997 and his M.S. and Ph.D. in physics from Brown University in 1999 and 2003, respectively. He has authored or co-authored eleven articles and holds one patent in the field of magnetic sensors and imaging. His work on high-resolution magnetic field imaging for fault isolation earned him a Most Outstanding Paper at ISTFA 2003. His current research interests include the application of magnetic imaging to semiconductor devices, novel magnetic materials and devices, and spintronics.

Xiaoyong Liu is the project manager of magnetic sensor development at Micro Magnetics. He received a B.S. and M.S. in crystal physics from Nanjing University in 1995 and 1998, respectively, and an M.S. and Ph.D. in physics from Brown University in 2000 and 2004. He is the author or co-author of twelve articles and holds one patent in the areas of magnetism and magnetic sensors. His work on high-resolution magnetic field imaging for fault isolation earned him a Most Outstanding Paper at ISTFA 2003. His research interests include magnetic tunnel junction sensors, magnetic device fabrication and characterization, and micromagnetic simulations.

Jan S. Hoftun is the senior software engineer at Micro Magnetics. He received his Cand.Mag. in physics from the University of Bergen in Norway in 1976. Jan received an M.S. and Ph.D. in physics from The Ohio State University in 1979 and 1983, respectively. After twelve years as an assistant professor of physics at Brown University, he joined Zeller Research, where he worked as a senior software engineer from 1996 until 2002. He joined Micro Magnetics in 2002. Dr. Hoftun is the author of over 100 articles in the field of experimental high-energy physics. He is a leading expert in cutting-edge data acquisition hardware and software. His research interests include high-speed data acquisition hardware and software and control systems for advanced robotic manufacturing machines.

Peter L. Klinger graduated from Vermont Technical College with an Associates Degree in electrical and electronics engineering in computer technology in 1990. He then joined IBM in East Fishkill, N.Y., in the Advanced Semiconductor Technology Center in yield/defect diagnostics. In 1992, he left to pursue a career in quality control and quality control management. In 1999, he rejoined IBM in Burlington as a failure analysis technician in logic analysis in the IBM Systems and Technology Group, OEM.

About the Authors *(continued)*

Theodore M. Levin is a staff engineer with the IBM Systems and Technology Group, which he joined in 1999. He received his B.S. in physics from the University of Massachusetts at Amherst in 1990. He received his M.S. in physics in 1994 and his M.S.E.E. in 1999, both from The Ohio State University. He has authored several articles in the fields of semiconductor materials characterization, failure analysis, and reliability. He holds one U.S. patent. His current research activities focus on improvement and applications of laser signal injection microscopy.

David P. Vallett received the BSEE degree from SUNY Buffalo in 1982. Since then he has been with the IBM Systems and Technology Group in Essex Junction, Vt., in both management and engineering positions in CMOS characterization and failure analysis. He is currently responsible for failure analysis technology development. He has authored several articles in the field, received four best-paper awards, and has given a number of invited talks and lectures on failure analysis technology challenges in micro- and nanoelectronics. He holds eleven U.S. patents and was given IBM's Outstanding Technical Achievement award for his work on picosecond imaging circuit analysis (PICA). He is a member of IEEE; Tau Beta Pi, the National Engineering Honor Society; EDFAS; and past chair of the International SEMATECH Product Analysis Forum. His current research activities are submicron current-density imaging using SQUID and magnetoresistive sensors, and x-ray tomography for subsurface defect imaging.